Binary fluid convection in a rotating cylinder

Marta Net, Isabel Mercader, and Edgar Knobloch

Citation: Phys. Fluids **7**, 1553 (1995); doi: 10.1063/1.868542
View online: http://dx.doi.org/10.1063/1.868542
View Table of Contents: http://pof.aip.org/resource/1/PHFLE6/v7/i7
Published by the AIP Publishing LLC.

Binary fluid convection in a rotating cylinder

Marta Net and Isabel Mercader
Departament de Física Aplicada, Universitat Politècnica de Catalunya, 08034 Barcelona, Spain

Edgar Knobloch
Department of Physics, University of California, Berkeley, California 94720

(Received 28 December 1994; accepted 14 March 1995)

The onset of convection in binary fluid mixtures in a rotating vertical cylinder is considered. Parameter values and boundary conditions relevant to experiments on ^{3}He–^{4}He mixtures with negative separation ratio are used. The eigenfunctions take the form of rigidly precessing spirals. The azimuthal wavenumber of the first unstable mode as the Rayleigh number increases is calculated as a function of the rotation rate and the separation ratio, as are the critical Rayleigh numbers and precession frequencies. Depending on the parameters the spirals may take the form of spatially extended body modes which fill the container, or of wall modes confined to its boundary. The former typically precess in the retrograde direction, while the latter are prograde. Under appropriate circumstances the binary system with a negative separation ratio becomes unstable for lower Rayleigh numbers than a pure fluid. This property of the system is enhanced by the wall modes. © *1995 American Institute of Physics.*

I. INTRODUCTION

Recent experiments[1–3] on convection in a pure fluid confined to a vertical cylinder heated from below and rotating uniformly about its axis have revealed several new features. The most interesting is that near onset convection takes the form of rigidly precessing spirals. These spirals are localized near the wall of the cylinder, and we call them wall modes. Numerical computations of critical Rayleigh numbers, precession frequencies and azimuthal wavenumbers are in good agreement with the experimental values.[4,5] In addition to describing the wall modes the theory can also be used to obtain a different class of eigenfunctions called body modes. In contrast to the wall modes these modes fill the container and precess substantially more slowly. The wall modes are the preferred modes at larger rotation rates while the body modes dominate at low rotation rates. The competition between these two types of modes is complex and is discussed in detail by Goldstein *et al.*[4,5]

The pure fluid problem is in one respect unsatisfactory. This is because rotation is required for the presence of overstability; in the absence of rotation there are no oscillations. In contrast, in systems such as binary fluid mixtures with a sufficiently negative separation ratio, oscillations can take place even in a nonrotating cylinder. Consequently such a system is ideal for the study of the effects of slow rotation on such oscillations, and in particular the resulting rotational mode splitting. On the basis of abstract theory we know that when the rotation rate Ω vanishes convection in the weakly nonlinear regime can take the form of either standing waves or of travelling waves that propagate either clockwise or counterclockwise around the cylinder. The term standing waves (hereafter SW) is used here to indicate the absence of azimuthal propagation; an SW eigenfunction can take the form of a wave travelling radially outwards.[6] When the reflection symmetry in vertical planes is broken by the rotation SW are no longer possible; instead the initial instability takes the form of *either* clockwise or counterclockwise travelling waves (hereafter TW). The counterpart of the SW is now a modulated travelling wave (MW) that bifurcates in a secondary bifurcation from the branch of either the clockwise or counterclockwise travelling waves.[7]

The present paper is concerned with the onset of convection in binary fluid mixtures with negative separation ratios in a uniformly rotating cylinder. We focus on the effects of rotation on the multiplicity of modes and the process of mode selection described for the nonrotating system by Mercader *et al.*[6] The system displays a number of new features involving the transition from body modes to wall modes that are absent in the unbounded problem.[8] In addition we confirm the presence of the destabilizing effect of a negative separation ratio, first predicted theoretically for an unbounded system by Masuda[9] and Pearlstein.[10]

The paper is organized as follows. In Sec. II we formulate the hydrodynamical equations and describe the technique we use to solve them. In Sec. III we describe the results of our computations. Section IV describes the theoretical interpretation of these results, while their implications are discussed in the final section.

II. FORMULATION AND METHOD OF SOLUTION

We consider Boussinesq binary fluid convection in a right circular cylinder of height h and radius Γh. The nondimensional equations describing the onset of instability as the Rayleigh number R is increased are given by[4,6]

$$\frac{1}{\sigma}\frac{\partial \mathbf{u}}{\partial t}+2\boldsymbol{\Omega}\times\mathbf{u}=-\nabla p+R(\Theta+S\Sigma)\hat{z}+\nabla^2\mathbf{u}, \tag{1a}$$

$$\frac{\partial \Theta}{\partial t}=w+\nabla^2\Theta, \tag{1b}$$

$$\frac{\partial \Sigma}{\partial t}=w+\tau\nabla^2\Sigma-\tau\nabla^2\Theta, \tag{1c}$$

[a]E-mail: knobloch@physics.berkeley.edu

$$\nabla \cdot \mathbf{u} = 0. \tag{1d}$$

Here Ω is the rotation rate in units of the vertical viscous diffusion time, S is the separation ratio, τ the Lewis number and σ the Prandtl number. The quantities Θ and Σ denote, respectively, the temperature and concentration perturbations relative to their conduction profiles, while $\mathbf{u}=(u,v,w)$ is the velocity perturbation in cylindrical coordinates (r,ϕ,z). In writing equations (1) we have assumed that the Froude number $\Gamma h\Omega^2/g \ll 1$ so that effective gravity continues to act vertically. We consider two types of boundary conditions,

$$\frac{\partial u}{\partial z} = \frac{\partial v}{\partial z} = w = \Theta = \frac{\partial \Theta}{\partial z} - \frac{\partial \Sigma}{\partial z} = 0 \quad \text{on } z=0,1, \tag{2a}$$

$$\mathbf{u} = \frac{\partial \Theta}{\partial r} = \frac{\partial \Sigma}{\partial r} = 0 \quad \text{on } r=\Gamma \tag{2b}$$

and

$$\mathbf{u} = \Theta = \frac{\partial \Theta}{\partial z} - \frac{\partial \Sigma}{\partial z} = 0 \quad \text{on } z=0,1, \tag{3a}$$

$$\mathbf{u} = \frac{\partial \Theta}{\partial r} = \frac{\partial \Sigma}{\partial r} = 0 \quad \text{on } r=\Gamma. \tag{3b}$$

Both sets of boundary conditions describe a no-slip no-flux boundary at $r=\Gamma$, with fixed temperature no-mass-flux boundary conditions at the top and bottom, which are stress-free in the former and no-slip in the latter. In the following we refer to these for short as stress-free and rigid. We emphasize, however, that due to the no-mass-flux boundary conditions at top and bottom the stress-free problem is, like the rigid problem, non-separable. In the calculations reported below we solve the former using a Galerkin method in the vertical, and the latter using a Chebyshev collocation method. In both cases the collocation method is used in the radial direction.[4,11] The formulation of the eigenvalue problem is completed by imposing an appropriate regularity condition at $r=0$.[11,12]

We seek solutions of the form $f(r,\phi,z,t) = F(r,z)e^{i(m\phi+\omega t)}$, where $F(r,z)$ depends on the chosen value of m. The (nonseparable) eigenvalue problem in (r,z) is solved for each m, and yields the critical Rayleigh number $R_c^{(m)}$ and the corresponding Hopf frequency $\omega_c^{(m)}$, for fixed values of τ, σ, S and Γ. Note that $\omega_c^{(m)}<0$ for modes that travel counterclockwise, while $\omega_c^{(m)}>0$ for clockwise modes; the former will be referred to as *prograde* frequencies and the latter as *retrograde*. By minimizing $R_c^{(m)}$ over m it is possible to identify the azimuthal wavenumber of the mode that first sets in.

III. RESULTS

Most of the results reported in the following are for a $\Gamma=2.76$ container and $\tau=0.067$, $\sigma=0.755$, the parameter values appropriate to an ongoing experiment by Lucas and coworkers[13,14] using ^{3}He–^{4}He mixtures at cryogenic temperatures. In Fig. 1 we show the results for (a) the critical Rayleigh numbers $R_c^{(0)}$ and (b) the corresponding frequencies $\omega_c^{(0)}$ as a function of the dimensionless rotation rate Ω for several values of S and the boundary conditions (2a,b).

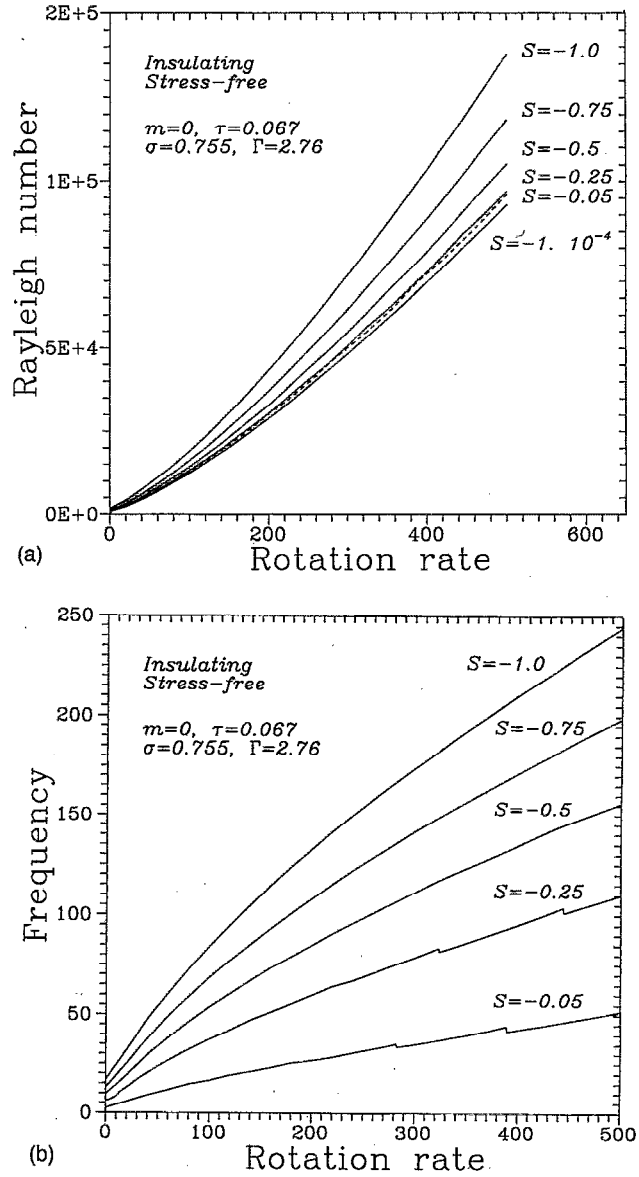

FIG. 1. (a) $R_c^{(0)}(\Omega)$ and (b) $\omega_c^{(0)}(\Omega)$ for $\Gamma=2.76$, $\tau=0.067$, $\sigma=0.755$ for different values of S and the boundary conditions (2a,b). In (a) the broken line represents the result for $S=-0.05$.

Since the mode is axisymmetric it is a body mode and it does not precess. For small Ω these oscillations are entirely due to doubly diffusive overstability; the Prandtl number is not small enough to produce axisymmetric oscillations dominated by a restoring force due to the Coriolis force. With increasing Ω the oscillations quickly take on the character of inertial oscillations. The jumps in $\omega_c^{(0)}$ arise when one radial $m=0$ mode supersedes another; only the lowest $R_c^{(0)}$ mode is shown. Figure 2 shows $R_c^{(m)}$ and $\omega_c^{(m)}$ as functions of Ω for $S=-0.25$. In (a) the broken line shows the corresponding $m=0$ result. Note that throughout nearly the whole range of Ω shown it is a nonaxisymmetric (i.e., precessing) mode that is the mode that first becomes unstable. As the rotation rate increases the critical Rayleigh numbers for the nonaxisymmetric modes increase with Ω but substantially more slowly

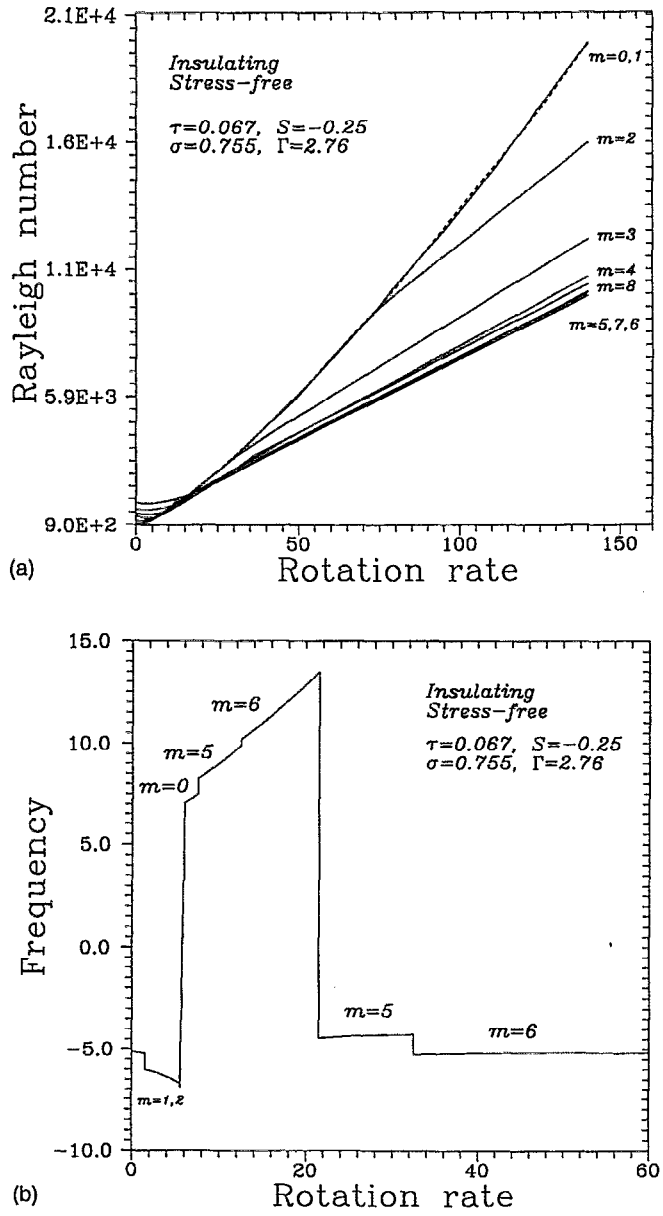

FIG. 2. (a) $R_c^{(m)}(\Omega)$ and (b) $\omega_c^{(m)}(\Omega)$ for $\Gamma=2.76$, $\tau=0.067$, $\sigma=0.755$, $S=-0.25$ and different values of the azimuthal wavenumber m. In (a) the broken line represents the case $m=0$. Only the lowest mode is shown for each m.

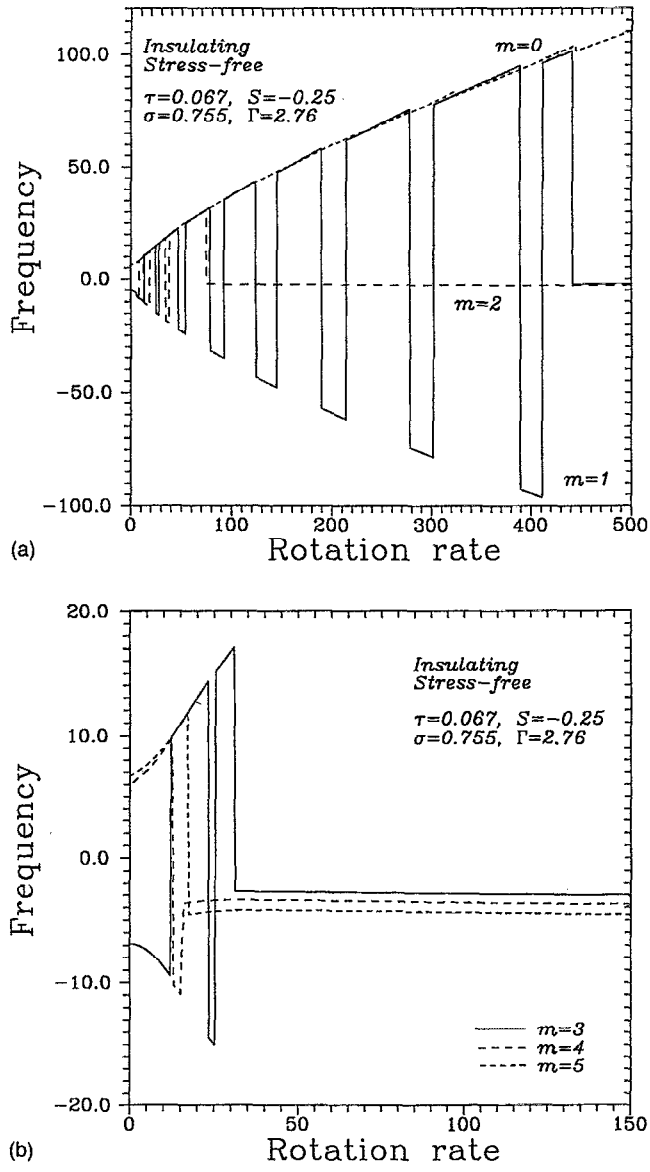

FIG. 3. Oscillation frequencies $\omega_c^{(m)}(\Omega)$ for prograde ($\omega_c>0$) and retrograde ($\omega_c<0$) modes with the same wavenumbers m and parameter values corresponding to those of Fig. 2. (a) $0\leqslant m\leqslant 2$, (b) $3\leqslant m\leqslant 5$.

than for the axisymmetric mode. This is similar to the situation that arises in a pure fluid,[4] and indicates that the sidewalls have a destabilizing effect. This effect is present because the boundaries can support a new type of mode called a wall mode. In a pure fluid these wall modes are nonaxisymmetric and typically precess counter to the direction of rotation of the cylinder with relatively high precession frequencies, in contrast to the body modes which precess more slowly.[4] In such a system the body modes are preferred at low rotation rates, but are superseded by the wall modes at larger Ω. In the present system the modes for $\Omega<7.5$ are all body modes, but due to the stabilizing concentration gradient ($S<0$) the oscillation frequency is relatively high. For larger rotation rates the problem begins to differ totally from the corresponding pure fluid problem. The selected mode has a low *prograde* frequency instead of a large retrograde frequency. Moreover there is no mode selection with increasing Ω: the selected mode remains $m=6$ even for very high Ω. Examination of the structure of this mode indicates that this mode is nonetheless a wall mode. Its character is, however, entirely different from that of the wall modes in a pure fluid, as indicated by the constancy of the precession frequency with increasing Ω. In Sec. IV we indicate that just such prograde modes are to be expected if the Poincaré equation for a rotating cylinder is generalized to include the effects of a stabilizing stratification. Here such a stratification develops in response to the applied destabilizing temperature gradient because $S<0$. In Fig. 3 we show the competition between different modes with the same azimuthal wavenumber m as Ω varies. For small Ω the lowest lying mode is alternately a

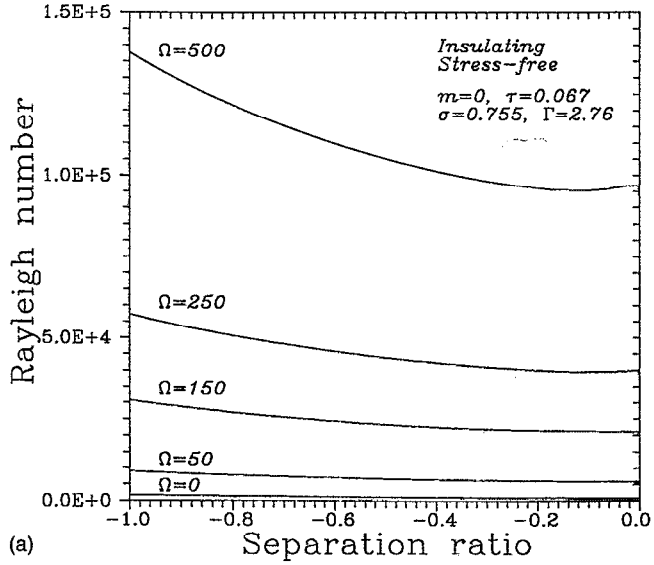

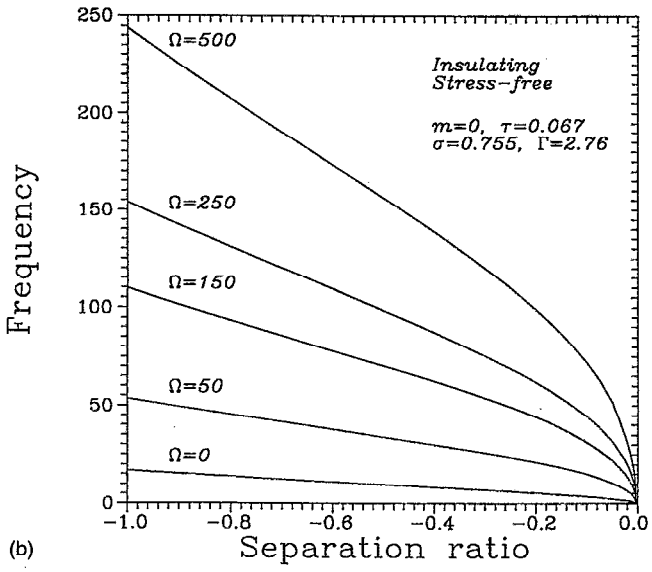

FIG. 4. (a) $R_c^{(0)}(S)$ and (b) $\omega_c^{(0)}(S)$ for $\Gamma=2.76$, $\tau=0.067$, $\sigma=0.755$ and different values of Ω.

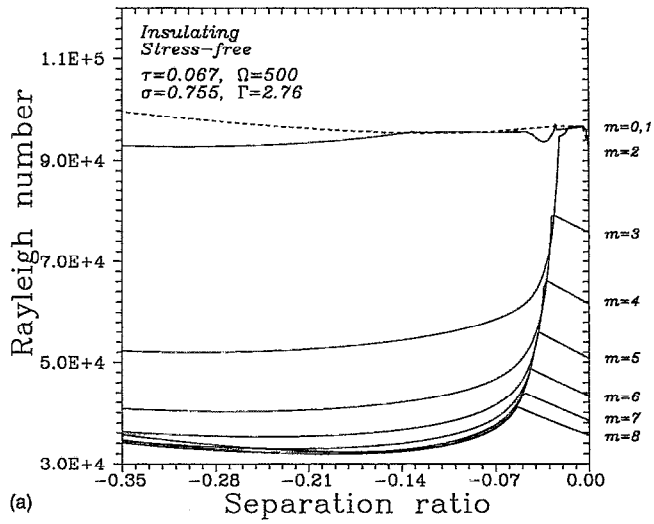

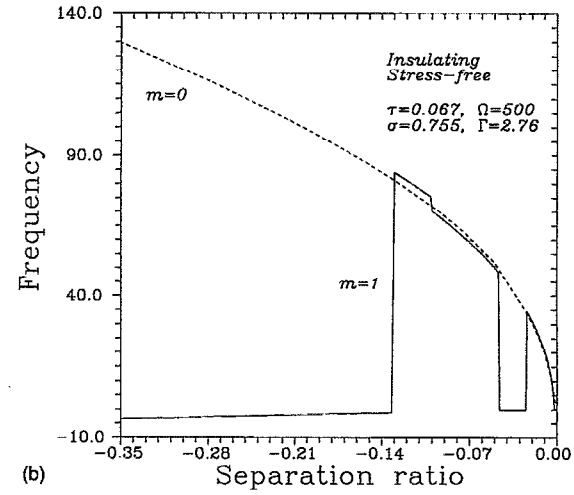

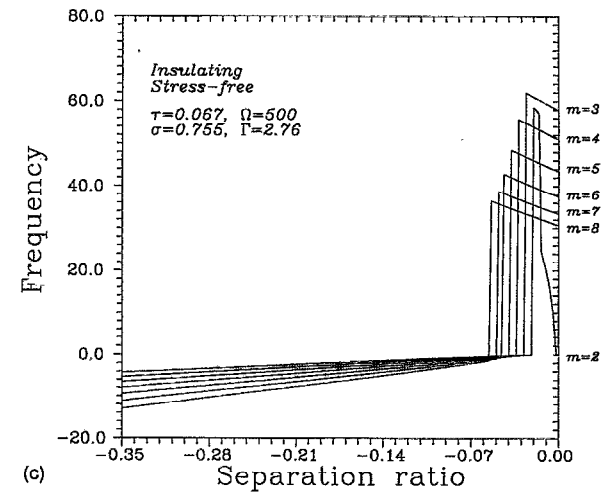

FIG. 5. (a) $R_c^{(m)}(S)$ and (b) $\omega_c^{(m)}(S)$ for $\Gamma=2.76$, $\tau=0.067$, $\sigma=0.755$ and $\Omega=500$. (c) shows $\omega_c^{(m)}(S)$ for $m\geq 2$. Note the abrupt decrease of $R_c^{(m)}$ with increasing $|S|$ and the corresponding transition to prograde modes.

prograde and retrograde body mode, although with increasing Ω there is a transition to a prograde wall mode. For $m<5$ this transition occurs at smaller Ω as m increases while for $m\geq 5$ the corresponding Ω increases again. As before there is no axisymmetric wall mode.

In Fig. 4 we turn to the separation ratio dependence of the above results, and through that to another novel characteristic of the present system. The figure shows $R_c^{(0)}(S)$ and $\omega_c^{(0)}(S)$ for stress-free boundary conditions and several values of Ω. Observe that $R_c^{(0)}(S)$ actually decreases with increasing $|S|$ in a range of S, i.e., in this range increasing the stable stratification leads to a *lowering* of the threshold for instability. This phenomenon, first described for an unbounded system by Masuda[9] and Pearlstein[10] and explained by Acheson,[15] requires that $\sigma<1<\sigma/\tau$ as well as a sufficiently high rotation rate, here approximately $\Omega>250$. In contrast $\omega_c^{(0)}(S)$ remains monotonic. As in the rotating pure fluid problem the axisymmetric problem is the one that approximates the theory for an unbounded layer the closest.

Figure 5 shows that the above results change dramatically due to the presence of the nonaxisymmetric wall modes. In particular for the dominant mode for our parameter values ($m=6$ at $S=-0.25$), the destabilization is much more pronounced and takes place over a much larger interval in S. In fact the effect is even more striking for a nonaxisymmetric mode such as $m=2$, even though this mode is never the first to go unstable. In Figs. 5(b), 5(c) we show graphically that the decrease in the stability of the system is due to the onset of the prograde wall modes. Such modes are of course absent in the unbounded layer discussed in Ref. 8. Figure 6 demonstrates the effect of even weak rotation on the selection between prograde and retrograde modes. Recall that when $\Omega=0$ the prograde and retrograde modes with the same azimuthal wavenumber are related by reflection symmetry and hence have the same frequencies and critical Rayleigh numbers. However, this degeneracy is broken as soon as $\Omega\neq 0$. Fig. 6(b) shows that the retrograde mode (solid line) is preferred for small $|S|$, while the prograde mode (broken line) is selected for larger $|S|$. Note that the critical Rayleigh number for the prograde mode diverges at a finite S as $|S|$ decreases; this is because a pure fluid can only support retrograde modes for this value of the Prandtl number (cf. Refs. 4, 5). In contrast, the critical Rayleigh number for the retrograde mode decreases rapidly as $|S|\rightarrow 0$ as the frequency of the mode changes from being of the order of the buoyancy frequency to being comparable to the rotation frequency. In fact one recognizes in Fig. 6(b) an "unfolding" of the neutral stability curves for Hopf and steady state instabilities around the Takens-Bogdanov point,[5] the nearly vertical portions of the curves arising from what was the steady state curve when $\Omega=0$, while the other parts of the curves come from the rotational splitting of the Hopf curve [see Fig. 6(a)].

In Fig. 7 we present results for the rigid boundary conditions (3a,b) and parameter values appropriate to the experimental values of Lucas *et al.*[13,14] Figure 7(a) shows $R_c(\Omega)$ for $\Gamma=2.76$, $\tau=0.025$, $\sigma=0.547$ and $S=-9.1\times 10^{-5}$, while Figs. 7(b), 7(c) show the corresponding precession frequencies. Not surprisingly, these results are similar to those for a pure fluid. In Fig. 8 we show the corresponding results for $\Gamma=2.76$, $\tau=0.067$, $\sigma=0.755$ and several values of S chosen to exhibit the type of behavior already seen with the stress-free boundaries. The details, such as the sequence of transitions with increasing Ω differ, however, as do the wavenumbers selected at larger Ω: for example for $S=-0.288$ the $m=7$ mode is selected for the rigid boundaries and $m=6$ for the stress-free ones. This difference could be due to the different boundary conditions used in these two calculations or to the slightly different parameter values. In Fig. 8(a) we also present the critical Rayleigh numbers for the axisymmetric modes (dashed lines) since these are the only modes that survive in the unbounded system. We see that for these modes the effect of increasing $|S|$ (typically) raises the critical Rayleigh number, regardless of the rotation rate. This is in contrast to the nonaxisymmetric wall modes for which increasing $|S|$ reduces the critical Rayleigh number once the rotation is sufficiently high. This is in addition to the fact that for fixed S sufficiently large rotation rates also lower the critical Rayleigh number relative to that for the axisymmetric

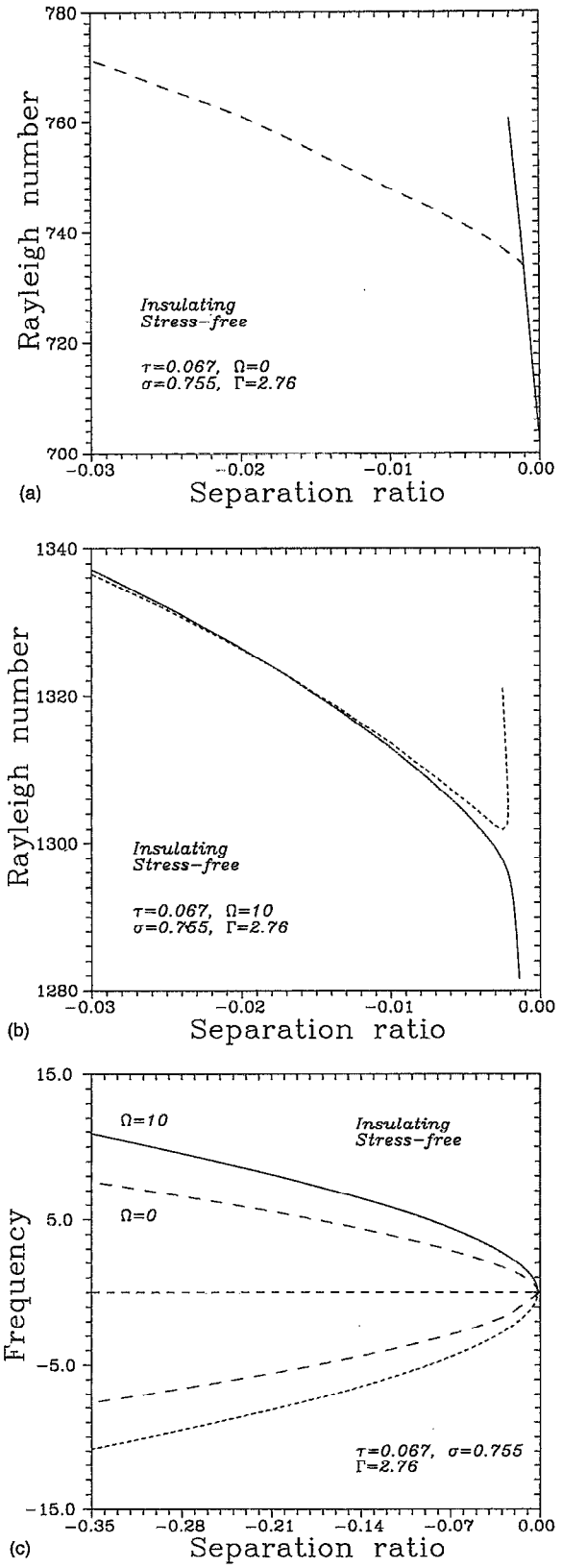

FIG. 6. $R_c^{(1)}(S)$ for $\Gamma=2.76$, $\tau=0.067$, $\sigma=0.755$ and (a) $\Omega=0$, (b) $\Omega=10$, showing the effects of rotational mode splitting. In (a) the solid (broken) line corresponds to steady state (oscillatory) instability; in (b) there are no steady state instabilities and the solid (broken) line corresponds retrograde (prograde) modes. (c) shows the corresponding frequencies $\omega_c^{(1)}$. Although not visible in the figure $\omega_c^{(1)}$ is symmetrical about $\omega=0$ when $\Omega=0$ but asymmetrical when $\Omega=10$. Note the sensitive dependence of $R_c^{(1)}$ on Ω.

modes. As already mentioned this effect is due to the presence of the wall modes and occurs even in a pure fluid. In Fig. 9 we show the effect of rotation on the $m=7$ mode. At $\Omega=0$ the prograde and retrograde modes have the same frequency, the buoyancy frequency. However, with increasing Ω the precession frequency of the retrograde mode increases while that of the prograde mode decreases. As a consequence the critical Rayleigh number for the prograde mode falls below that for the retrograde mode, and the prograde mode is selected [cf. Fig. 8(b)]. The dependence of these results on the separation ratio S is similar to that with the boundary conditions (2a,b) except that the rotation rate for which the destabilizing effect of the concentration gradient is first seen is increased, i.e., the rigid boundary conditions decrease the destabilizing effect of negative separation ratios. For example, when $m=0$ we find that $R_c^{(0)}$ increases monotonically with increasing $|S|$ even for $\Omega=500$, in contrast to Fig. 4(a).

In Fig. 10 we show a sequence of temperature eigenfunctions $\Re\Theta(r,z)e^{i(m\phi+\omega t)}$ at $z=\frac{1}{2}$ and several different rotation rates corresponding to Fig. 8. The eigenfunctions are shown in the comoving frame as a function of r and ϕ using two different representations. In each case the eigenfunction shown is the one that first loses stability at that rotation rate. Observe that the retrograde mode $m=8$ at $\Omega=30$ and the prograde mode $m=7$ at $\Omega=34$ have very similar structure. Nonetheless, because rotation favors retrograde motion while stabilizing stratification favors prograde motion the former mode appears to be rotation dominated and the latter stratification dominated. As with the stress-free boundary conditions the modes that are first unstable are nearly always wall modes, and they come in at Rayleigh numbers substantially lower than those required for the destabilization of an axisymmetric body mode. In this respect the situation is quite similar to that occurring in a pure fluid.

A vertical section of the $\Omega=30$ and $\Omega=34$ eigenfunctions at fixed r $(0<r<\Gamma)$ shows that the waves lead at midlevel with the points near $z=0,1$ trailing behind. More generally the eigenfunction curvature depends both on r and on the system parameters, and may even change sign with increasing r $(0<r<\Gamma)$. This is because the eigenfunction can be written in the form

$$\Re\Theta(r,z)e^{i(m\phi+\omega t)}=|\Theta(r,z)|\cos[m\phi+\omega t+\Phi(r,z)]. \quad (4)$$

In general a mode of this form propagates *both* in the azimuthal and radial directions, and hence takes the form of a rigidly rotating *spiral* (cf. Fig. 10). The phase $\Phi(r,z)$ differs for the different fields Θ, Σ, u, v, w and it is these phase lags that are responsible for the propagation of the wave.[16,17] Similar behavior is present already in the two-dimensional plane layer as soon as realistic boundary conditions are imposed at the top and bottom.[18]

IV. THEORETICAL INTERPRETATION

In this section we discuss theoretically some of the properties of the unstable modes that follow from straightforward considerations. We begin by considering the mode structure in an *ideal* but stratified fluid confined in a rotating cylinder. This analysis leads to a qualitative understanding of many of

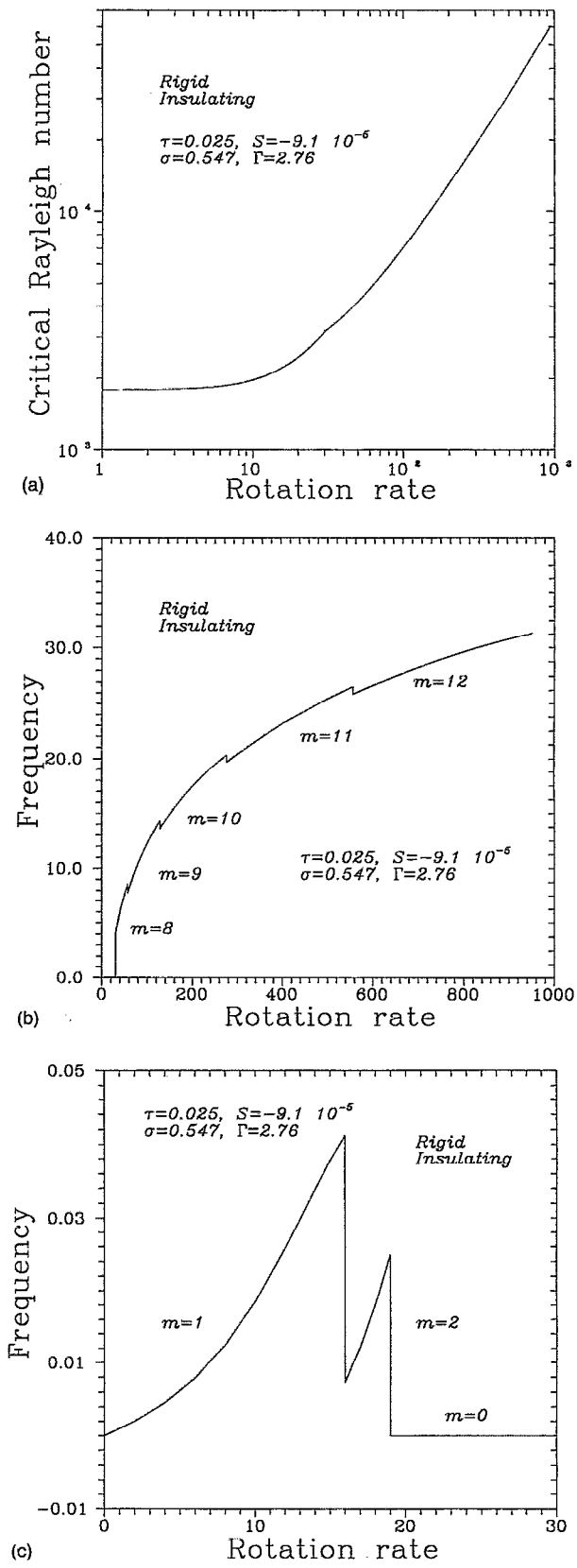

FIG. 7. (a) $R_c(\Omega)$ and (b) $\omega_c(\Omega)$ for $\Gamma=2.76$, $\tau=0.025$, $\sigma=0.547$, $S=-9.1\times10^{-5}$ and the boundary conditions (3a,b). (c) shows a detail of (b).

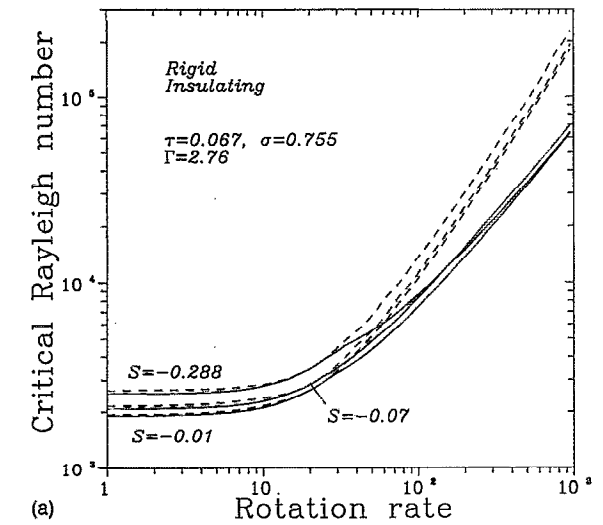

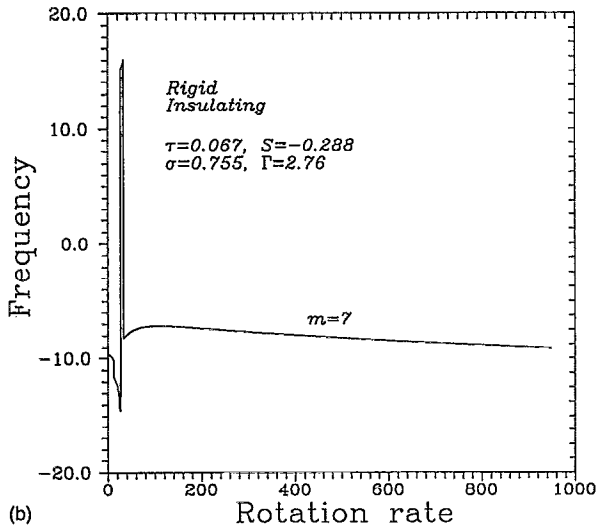

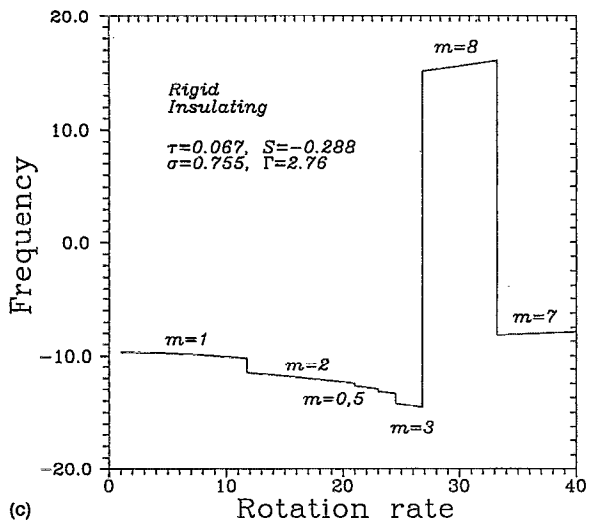

FIG. 8. (a) $R_c(\Omega)$ and (b) $\omega_c(\Omega)$ for $\Gamma=2.76$, $\tau=0.067$, $\sigma=0.755$, $S=-0.288$ and the boundary conditions (3a,b). (a) shows $R_c(\Omega)$ for $S=-0.07$ and -0.01 as well (solid lines). Note the destabilizing effect of negative separation ratio at large Ω indicated by the crossing of the solid lines. The broken lines show the corresponding results for the axisymmetric mode $m=0$ in order to show (i) the destabilizing effect of rotation, and (ii) the (generally) stabilizing effect of negative separation ratio on this mode. (c) shows a detail of (b). For large rotation rates the prograde $m=7$ mode is selected.

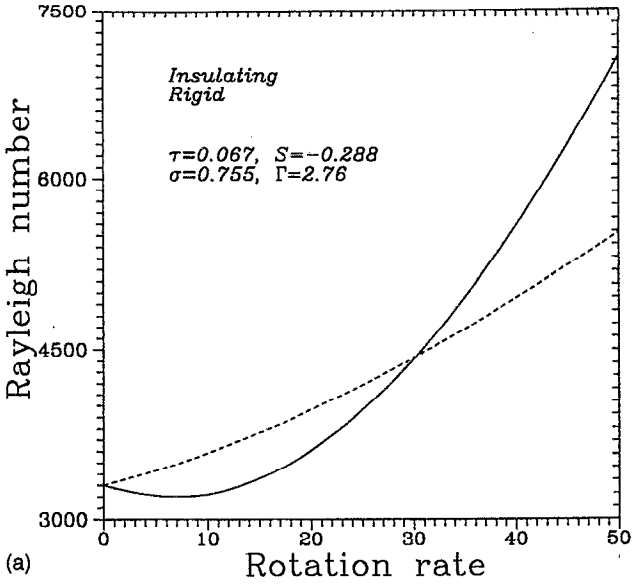

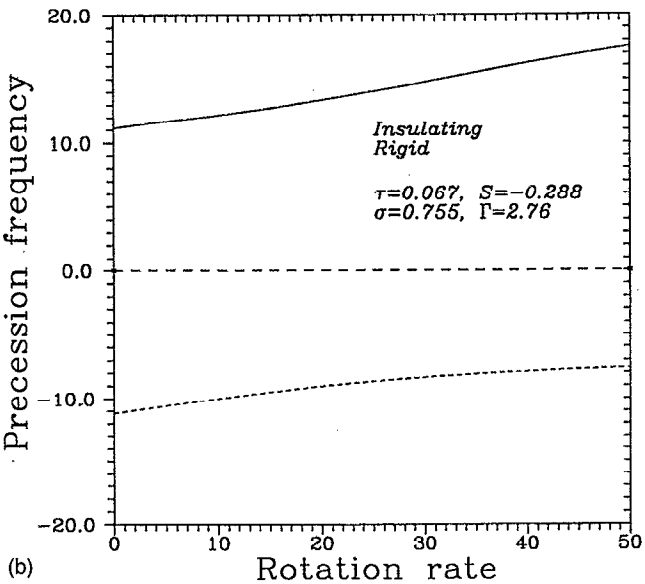

FIG. 9. (a) $R_c^{(7)}(\Omega)$ and (b) $\omega_c^{(7)}(\Omega)$ for $\Gamma=2.76$, $\tau=0.067$, $\sigma=0.755$ and $S=-0.288$, showing the effects of rotational mode splitting. The solid (broken) line corresponds to retrograde (prograde) modes.

the results obtained in Sec. III. We then focus on understanding the destabilizing effect of negative separation ratios. Finally we discuss, following[19,20] a simplified model consisting of a rotating fluid-filled semi-infinite domain bounded by a straight boundary, and use this model to identify semi-analytically unstable modes in the form of wall modes.

A. The dissipationless problem

We begin by considering the dissipationless system. We suppose that there are two competing contributions to the density stratification, arising from, say, thermal and solutal stratification. These affect the density in opposite ways, but in the absence of dissipation no diffusive instabilities can take place. Consequently the dynamics of the system are

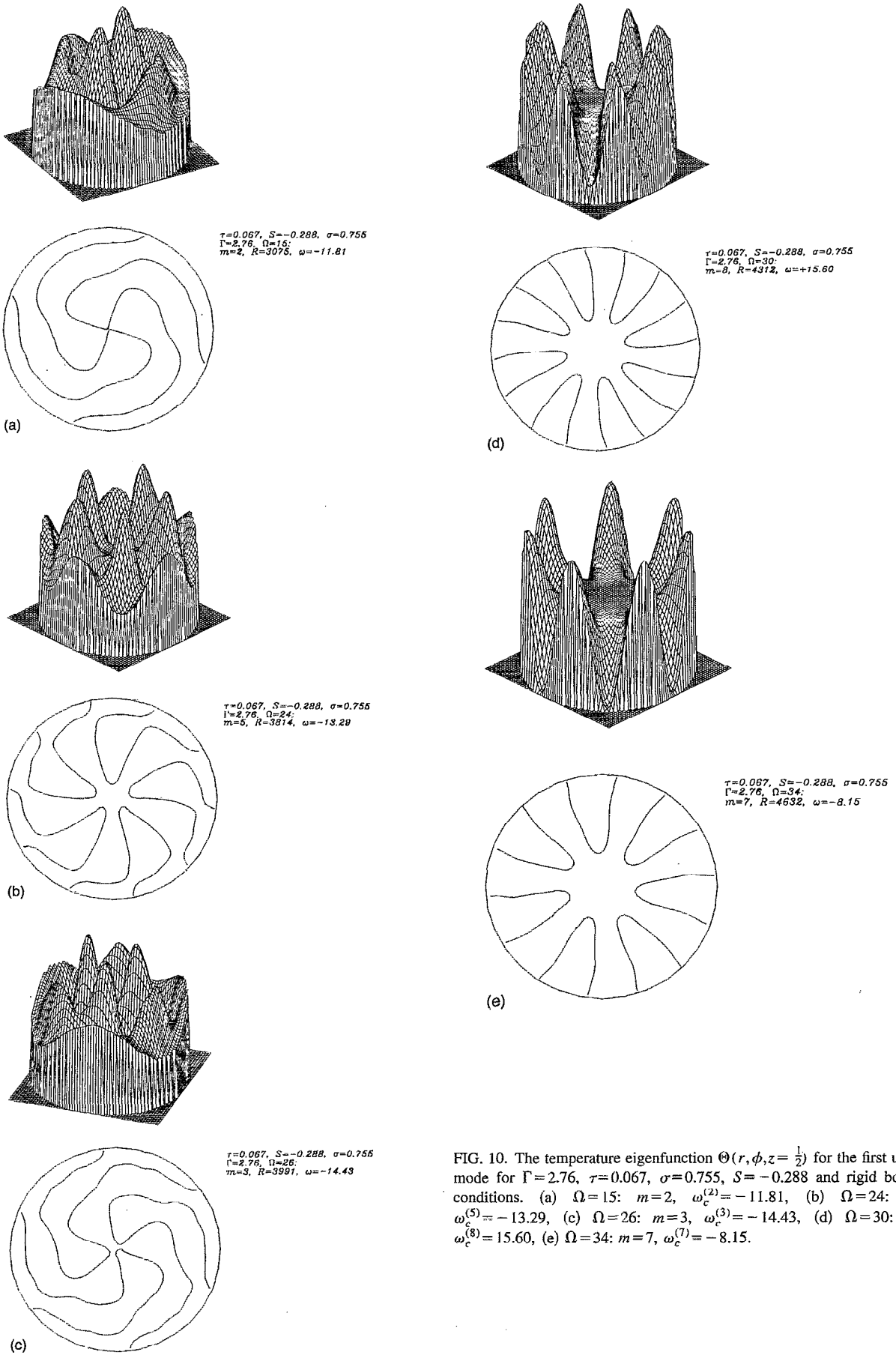

FIG. 10. The temperature eigenfunction $\Theta(r,\phi,z=\frac{1}{2})$ for the first unstable mode for $\Gamma=2.76$, $\tau=0.067$, $\sigma=0.755$, $S=-0.288$ and rigid boundary conditions. (a) $\Omega=15$: $m=2$, $\omega_c^{(2)}=-11.81$, (b) $\Omega=24$: $m=5$, $\omega_c^{(5)}=-13.29$, (c) $\Omega=26$: $m=3$, $\omega_c^{(3)}=-14.43$, (d) $\Omega=30$: $m=8$, $\omega_c^{(8)}=15.60$, (e) $\Omega=34$: $m=7$, $\omega_c^{(7)}=-8.15$.

described by the overall density distribution which we take to be statically stable (density decreasing upwards). The overall density stratification is measured by the Brunt-Väisälä frequency $N \equiv \{-(g/\rho)(d\rho/dz)\}^{1/2}$ assumed to be real and positive. The natural time scale for the neutrally stable oscillations is then N^{-1} with velocities expressed in units of hN, where h is the height of the cylinder. The nondimensional equations take the form

$$\frac{\partial \mathbf{u}}{\partial t} + \frac{2}{N}\boldsymbol{\Omega}\times\mathbf{u} = -\nabla p + \frac{1}{N^2}(N_T^2\Theta - N_S^2\Sigma)\hat{z}, \tag{5a}$$

$$\frac{\partial \Theta}{\partial t} = w, \tag{5b}$$

$$\frac{\partial \Sigma}{\partial t} = w, \tag{5c}$$

$$\nabla\cdot\mathbf{u} = 0, \tag{5d}$$

where $N_T^2 = -g\alpha\,(\partial T_0/\partial z)$, $N_S^2 = -g\beta\,(\partial S_0/\partial z)$ and T_0 and S_0 are the (linear) temperature and concentration profiles in the basic state. Both T_0 and S_0 are assumed to decrease with height so that $N_T^2 > 0$, $N_S^2 > 0$. We look for infinitesimal oscillations with dimensionless frequency ω/N. The frequency ω is an eigenvalue of the problem

$$\nabla^2 p - \frac{4\Omega^2 - N^2}{\omega^2 - N^2}\frac{\partial^2 p}{\partial z^2} = 0 \tag{6}$$

specified by the boundary conditions $\mathbf{u}\cdot\mathbf{n} = 0$ on the boundaries of the cylinder. Here $N^2 \equiv N_S^2 - N_T^2$ and $\mathbf{n}$ is the outward normal to the surface. These boundary conditions correspond to stress-free fixed temperature and concentration boundary conditions at the top and bottom, with stress-free no-flux boundary conditions on the sides. These boundary conditions are the only ones compatible with the absence of dissipation.

Equation (6) with the above boundary conditions was analyzed in detail by Friedlander and Siegmann,[21] who pointed out that there are two distinct classes of modes, depending on whether the boundary value problem is elliptic or hyperbolic. Modes of class I satisfy $\min(4\Omega^2, N^2) < \omega^2 < \max(4\Omega^2, N^2)$, while those of class II satisfy $0 < \omega^2 < \min(4\Omega^2, N^2)$. We do not consider the degenerate cases $\omega^2 = \min(4\Omega^2, N^2)$ and $\omega^2 = 4\Omega^2 = N^2$. In either case the resulting eigenvalue problem is separable, and one may seek solutions of the form $p(r,\phi,z) = P(r)e^{im\phi}\cos n\pi z$, where $P(r)$ satisfies

$$\frac{1}{r}\frac{d}{dr}r\frac{dP}{dr} - \frac{m^2}{r^2}P - \frac{\omega^2 - 4\Omega^2}{\omega^2 - N^2}n^2\pi^2 P = 0, \quad n > 0, \tag{7}$$

$$P(0) = 0, \quad \frac{dP}{dr} + \frac{2\Omega m}{\omega r}P = 0 \ \text{ at } r = \Gamma. \tag{8}$$

For $m = 0$ the first condition is replaced by $P'(0) = 0$. It follows that class I solutions are given by

$$P(r) = J_m(\alpha r/\Gamma), \tag{9}$$

where

$$\omega^2 = \frac{\alpha^2 N^2 + 4\Omega^2 n^2\pi^2\Gamma^2}{\alpha^2 + n^2\pi^2\Gamma^2} \tag{10}$$

and α_{kmn} $(k = 1,2,\ldots)$ are the roots of $\omega\alpha J_m'(\alpha) + 2\Omega m J_m(\alpha) = 0$ and are real. The corresponding eigenfunctions oscillate in r and are similar to those in a pure fluid except for the modified frequency range. In our terminology these modes are body modes. In contrast class II modes are given by

$$P(r) = I_m(\alpha r/\Gamma), \tag{11}$$

where

$$\omega^2 = \frac{\alpha^2 N^2 - 4\Omega^2 n^2\pi^2\Gamma^2}{\alpha^2 - n^2\pi^2\Gamma^2} \tag{12}$$

and α_{mn} is now the root of $\omega\alpha I_m'(\alpha) + 2\Omega m I_m(\alpha) = 0$. Friedlander and Siegmann show that solutions of this problem correspond to internal waves that are confined to the wall of the cylinder (i.e., they are wall modes) and obtain the condition for such modes to exist. It is intuitively clear that this condition is equivalent to demanding that the rotation rate is sufficiently high, since no wall modes are present with no rotation. In addition they also show that modes of class II are always *prograde*, i.e., $\omega < 0$.[21]

These results are in qualitative agreement with those presented in Sec. III for the driven dissipative problem. In particular we see that the dissipative modes identified above are natural analogues of the body and wall modes present in the ideal problem. The results of Friedlander and Siegmann show, moreover, that the class II modes are only present if both $N > 0$, $\Omega > 0$, and that their (prograde) precession frequency is $\mathcal{O}(\Omega)$ if $2\Omega < N$, but is $\mathcal{O}(N)$ if $2\Omega > N$. This is again in qualitative agreement with our results for the dissipative case in which for sufficiently large Ω and fixed S the precession frequency of the critical wall modes was found to be both prograde and (essentially) independent of Ω. Once the precession frequencies of all nearby modes become independent of Ω there is no further mode crossing with increasing Ω, and hence no further mode selection, as seen in Fig. 8. Note that there are no type II modes when $N = 0$; consequently the wall modes described by Goldstein *et al.*[4] are intrinsically dissipative, and such modes are also present in our calculations when $|S|$ is sufficiently small. See also Ref. 6. The body modes are either inertial (if $2\Omega > N$) or internal waves (if $2\Omega < N$).

B. Stable stratification as a catalyst for instability

In this section we discuss the reason why the addition of bottom-heavy concentration can destabilize convection in a rotating layer. The explanation, suggested by Acheson,[15] ignores the presence of boundaries and consequently applies in the first instance only to axisymmetric modes. However, the explanation takes account of the various diffusive processes present in the system and hence complements the discussion in the preceding section of the modes of an ideal fluid in a bounded container.

The basic idea is as follows. Consider a (rotating) pure fluid undergoing overstable oscillations. A necessary condition for the existence of such oscillations is that $\sigma < 1$,[5] although in an unbounded layer a more restrictive requirement can be obtained.[22] Acheson observes that the temperature

difference between a parcel of fluid oscillating with dimensionless frequency ω and its surroundings as it passes upwards through its equilibrium position is

$$\delta T = -A \frac{dT}{dz} \frac{\omega p}{\omega^2 + p^2}, \tag{13}$$

where A is the oscillation amplitude, dT/dz is the imposed (negative) temperature gradient and p is the square of the total wavenumber. For example, in a layer with idealized boundary conditions at top and bottom $p = \pi^2 + k^2$, where k is the horizontal wavenumber. Thus $\delta T > 0$ provided $\omega > 0$. An identical but negative temperature difference will be present on the downward path. These temperature changes are present because of a time lag between the velocity and temperature fields arising from thermal diffusion, and are necessary for the presence of overstability. From expression (13) it follows that δT is small if either ω is small or if ω is large. In the former case the oscillation frequency is so small that thermal diffusion keeps the parcel nearly in thermal equilibrium at all time, while in the latter case the frequency is so large that the parcel can exchange little heat with its surroundings during one oscillation. The largest δT arises in between, when $\omega = p$. Since the oscillation frequency is determined by the rotation rate Ω the system may be operating in a regime for which δT is not near maximum, and hence the extraction of energy from the thermal gradient is not optimal. In this case it is possible to destabilize the system by adding bottom-heavy solute that shifts the oscillation frequency towards optimal. If the solute diffuses slowly there will be no stabilizing effect due to solute diffusion into or out of the parcel during an oscillation. Thus the necessary condition for destabilization by a bottom-heavy gradient is

$$\tau < \sigma < 1. \tag{14}$$

In the remainder of this section we employ equations (1) with idealized boundary conditions at $z = 0,1$ to substantiate this physical picture.

In the system under consideration the bottom-heavy solute concentration develops in response to the applied temperature gradient, rather than being imposed externally. Since we are dealing with an unbounded layer it suffices to consider equations (1) in two dimensions:

$$\frac{1}{\sigma} \nabla^2 \frac{\partial \psi}{\partial t} = R\left(\frac{\partial \Theta}{\partial x} + S \frac{\partial \Sigma}{\partial x} \right) - 2\Omega \frac{\partial v}{\partial z} + \nabla^4 \psi, \tag{15a}$$

$$\frac{1}{\sigma} \frac{\partial v}{\partial t} = 2\Omega \frac{\partial \psi}{\partial z} + \nabla^2 v, \tag{15b}$$

$$\frac{\partial \Theta}{\partial t} = \frac{\partial \psi}{\partial x} + \nabla^2 \Theta, \tag{15c}$$

$$\frac{\partial \Sigma}{\partial t} = \frac{\partial \psi}{\partial x} + \tau \nabla^2 \Sigma - \tau \nabla^2 \Theta \tag{15d}$$

subject to the boundary conditions

$$\psi = \frac{\partial^2 \psi}{\partial z^2} = \frac{\partial v}{\partial z} = \Theta = \Sigma = 0 \quad \text{on } z = 0,1. \tag{16}$$

Here ψ is the streamfunction. The properties of the resulting eigenvalue problem are described by the dispersion relation

$$\left(\frac{s}{\sigma} + p \right)^2 (s+p)(s+\tau p) - \frac{Rk^2}{p} \left(\frac{s}{\sigma} + p \right) \times [(1+S)s + p(\tau + S + \tau S)] + \frac{4\Omega^2 \pi^2}{p} (s+p)(s+\tau p) = 0, \tag{17}$$

where s is the growth rate of the instability. Consequently the critical value of R at marginal stability ($s = i\omega$, $\omega \neq 0$) is given by

$$R = \left[\frac{1}{\sigma}(\tau + S + \tau S) + 1 + S \right]^{-1} \left[\frac{p^3}{k^2} \left(1 + \tau + 2\frac{\tau}{\sigma} \right) - \frac{p}{k^2} \frac{\omega^2}{\sigma^2} (1 + \tau + 2\sigma) + (1+\tau) \frac{4\Omega^2 \pi^2}{k^2} \right]; \tag{18}$$

the frequency ω satisfies a quadratic equation for ω^2:

$$\frac{\omega^4}{\sigma^2} \left(1 + \frac{1}{\sigma} + S \right) - \frac{\omega^2}{\sigma} \left[\frac{4\Omega^2 \pi^2}{p} (1 - \sigma - \sigma S) - p^2 \left(1 + \sigma + \sigma S + \frac{1}{\sigma}(S + \tau^2 + \tau S + \tau^2 S) + \frac{\tau}{\sigma^2}(\tau + S + \tau S) \right) \right] + 4\Omega^2 \pi^2 p \left[S(1+\tau) + \tau^2 (1+S) - \frac{\tau}{\sigma}(\tau + S + \tau S) \right] + p^4 \left[S(1+\tau) + \tau^2 (1+S) + \frac{\tau}{\sigma}(\tau + S + \tau S) \right] = 0. \tag{19}$$

Equation (19) can have either one or two real solutions ω, depending on whether a primarily inertial or a primarily buoyancy oscillation is excited or both. As pointed out by Pearlstein[10] these two possibilities are of crucial importance since only in the latter case can a bottom-heavy solute cause an instability. One can check that in the case in which there are inertial oscillations ($\sigma < 1$) the condition (14) is necessary in order that equation (19) describes two modes of oscillation. That this is the same condition as obtained by Pearlstein for rotating doubly diffusive convection comes as no surprise: with idealized boundary conditions equations (1) can be transformed by a linear transformation into those studied by Pearlstein, *without* changing σ or τ.[23]

In order to check Acheson's picture of the instability we

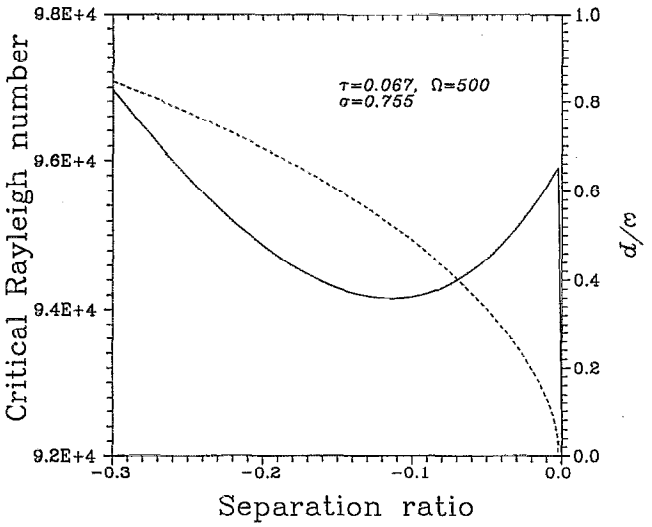

FIG. 11. The ratio ω/p (broken line) and the critical Rayleigh number R_c (solid line) as functions of S for an unbounded layer with idealized boundary conditions. The parameters are $\tau=0.067$, $\sigma=0.755$, and $\Omega=500$.

plot in Fig. 11 ω/p against S for $\tau=0.067$, $\sigma=0.755$ and $\Omega=500$. This plot is obtained by solving (19) for ω and using the p which minimizes the critical Rayleigh number at each value of S. On the same plot we show the corresponding R_c. One observes that the minimum in R_c at $S=-0.114$ occurs at $\omega/p=0.522$. Evidently in the present problem the agreement with the suggested criterion $\omega/p=1$ is significantly worse than in the example computed by Pearlstein.[10]

Not surprisingly the above picture also works for axisymmetric modes in a cylinder since these are approximated well by the modes of the unbounded system. For example, from Fig. 4 we see that for $\Omega=500$ the minimum value of R occurs at $S=-0.12$; the corresponding frequency is $\omega=79.8$. Acheson's criterion thus yields $p=79.8$, and this is to be compared with the following estimate of an effective p in a cylinder of aspect ratio $\Gamma=2.76$: $p\approx(n\pi/\Gamma)^2+\pi^2=139.4$. Here $n=10$ is the number of zeros in the $m=0$ eigenfunction at $S=-0.12$. Note that the ratio $\omega/p=0.57$ is similar to that for the unbounded layer. More surprising, however, is the fact Acheson's explanation also appears to work for the more dramatic destabilization involving the (nonaxisymmetric) wall modes. For example, Fig. 5 shows that when $\Omega=500$ the minimum Rayleigh number for the $m=2$ wall modes occurs at $S=-0.29$ while the corresponding frequency is $\omega^{(2)}=-3.50$. If we replace p by $\pi^2+m^2-\ell^2$, where ℓ measures the inverse decay length of the wall mode in the direction away from the wall, the criterion $\omega/p=1$ yields $\ell=5.11$. This result provides a reasonable estimate of the decay length of the computed eigenfunction. Note that for these modes $p<0$ (i.e., the modes are wall modes) and $\omega<0$ (the modes precess in the prograde direction). These properties are consistent with the physical requirement that $\delta T>0$.

C. Wall modes due to a straight boundary

In this section we consider a simplified form of the linear eigenvalue problem in a cylinder. Specifically we consider oscillations in a semi-infinite domain $\{-\infty<x<0, 0<z<1\}$ with a no-slip boundary placed at $x=0$ and free-slip boundaries at $z=0,1$. In addition we assume that the temperature and concentration are both maintained at constant values at the top and bottom. These boundaries have the advantage that they render the resulting eigenvalue problem separable. The resulting problem is much easier to study while retaining the essential physics of the problem, and enables us to check certain aspects of Acheson's destabilization mechanism more easily than in the bounded domain. Consequently we seek solutions of this problem in the form of wall modes[19,20] with an emphasis on the destabilizing effect of negative separation ratios noted in Sec. III. For the wall modes all fields are assumed to vanish exponentially as $x\to-\infty$. We start with equations (1) and look for solutions of the form $f(x,z)e^{i(my+\omega t)}$, where m is now a continuous wavenumber $(m\neq 0)$. With the boundary conditions chosen the problem is separable in z and hence $(u,v,w,\Theta,\Sigma,p)=(U(x)\cos\pi z, V(x)\cos\pi z, W(x)\sin\pi z, \Theta(x)\sin\pi z, \Sigma(x)\sin\pi z, P(x)\cos\pi z)$, where

$$\frac{i\omega}{\sigma}U=-DP+(D^2-m^2-\pi^2)U+2\Omega V, \tag{20a}$$

$$\frac{i\omega}{\sigma}V=-imP+(D^2-m^2-\pi^2)V-2\Omega U, \tag{20b}$$

$$\frac{i\omega}{\sigma}W=\pi P+R(\Theta+S\Sigma)+(D^2-m^2-\pi^2)W, \tag{20c}$$

$$i\omega\Theta=W+(D^2-m^2-\pi^2)\Theta, \tag{20d}$$

$$i\omega\Sigma=W+\tau(D^2-m^2-\pi^2)(\Sigma-\Theta), \tag{20e}$$

$$DU+\pi W=-imV. \tag{20f}$$

Eliminating the various fields in favor of W one now obtains

$$\left(D^2-m^2-\pi^2-\frac{i\omega}{\tau}\right)(D^2-m^2-\pi^2-i\omega)\left[\left(D^2-m^2-\pi^2-\frac{i\omega}{\sigma}\right)^2(D^2-m^2-\pi^2)-4\pi^2\Omega^2\right]W-R\left(D^2-m^2-\pi^2-\frac{i\omega}{\sigma}\right)$$

$$\times(D^2-m^2)\left[(D^2-m^2-\pi^2)\left(1+S+\frac{S}{\tau}\right)-\frac{1+S}{\tau}i\omega\right]W=0, \tag{21}$$

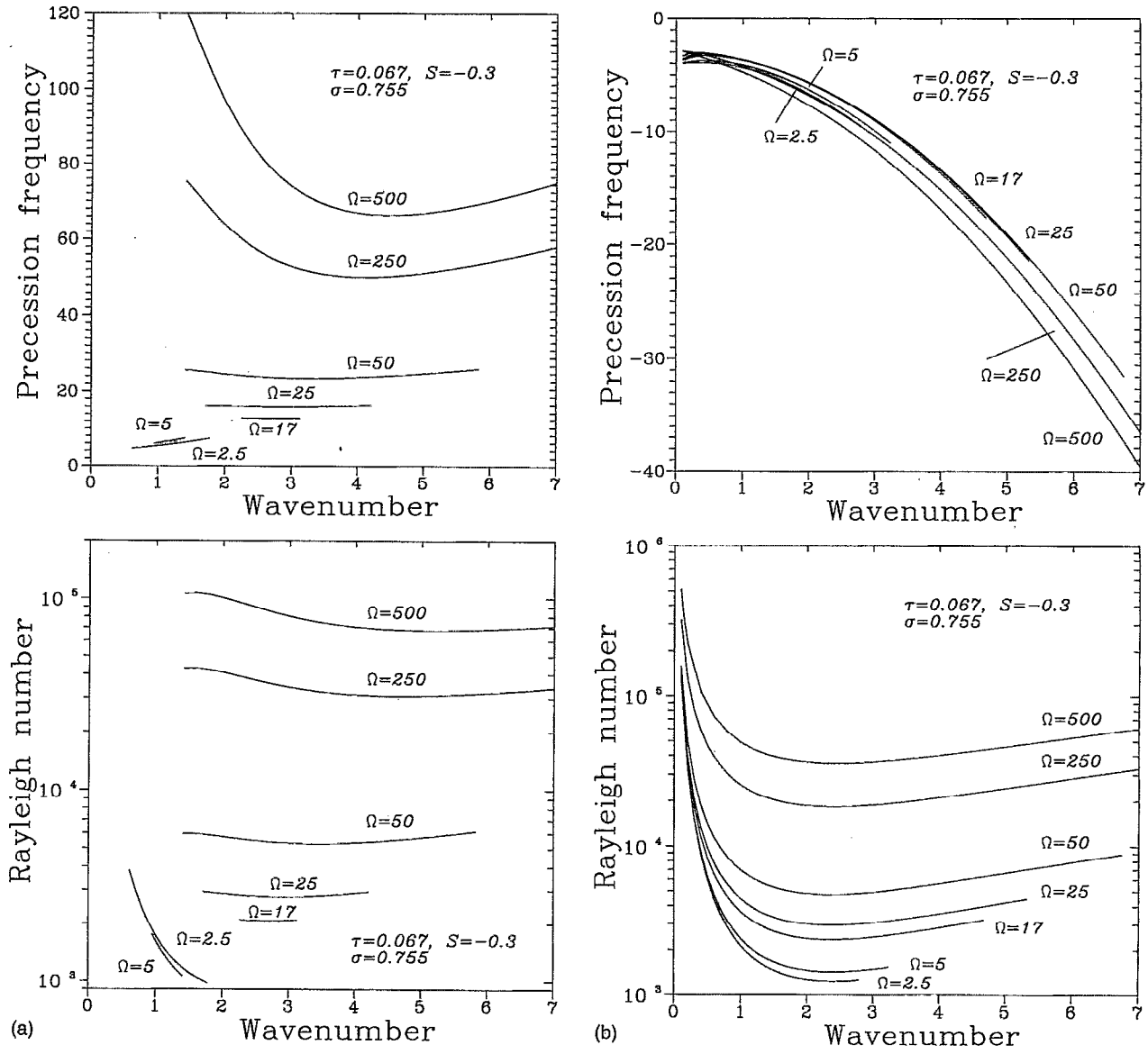

FIG. 12. Wall modes in the separable straight-wall model as a function of the azimuthal wavenumber m for $\tau=0.067$, $\sigma=0.755$, $S=-0.3$ and different values of Ω. (a) Retrograde modes, (b) prograde modes.

subject to the boundary conditions

$$U=V=W=D\Theta=D\Sigma=0 \quad \text{on } x=0 \tag{22}$$

and the requirement that the solutions vanish exponentially as $x\to-\infty$.

To find such solutions we suppose that $W(x)=e^{\lambda x}$ with $\Re\lambda>0$. It follows that

$$W(x)=\sum_{j=1}^{5} A_j e^{\lambda_j x}, \tag{23}$$

where $\lambda_j^2\equiv q_j+m^2+\pi^2$ and the q_j are the roots of the quintic

$$q\left(q-\frac{i\omega}{\sigma}\right)^2(q-i\omega)\left(q-\frac{i\omega}{\tau}\right)-R\left(q-\frac{i\omega}{\sigma}\right)(q+\pi^2)\times\left[q\left(1+S+\frac{S}{\tau}\right)-\frac{1+S}{\tau}i\omega\right]-4\pi^2\Omega^2(q-i\omega)\left(q-\frac{i\omega}{\tau}\right)=0. \tag{24}$$

The corresponding expressions for the remaining fields are readily found from equations (20):

$$U(x)=-\pi\sum_{j=1}^{5}\frac{A_j}{\lambda_j^2-m^2}\left(\lambda_j-\frac{2im\Omega}{\lambda_j^2-m^2-\pi^2-i\omega/\sigma}\right)e^{\lambda_j x}, \tag{25a}$$

$$V(x)=-\pi\sum_{j=1}^{5}\frac{A_j}{\lambda_j^2-m^2}\left(im+\frac{2\Omega\lambda_j}{\lambda_j^2-m^2-\pi^2-i\omega/\sigma}\right)e^{\lambda_j x}, \tag{25b}$$

$$D\Theta(x)=-\sum_{j=1}^{5}A_j\frac{\lambda_j}{\lambda_j^2-m^2-\pi^2-i\omega}e^{\lambda_j x}, \tag{25c}$$

$$D\Sigma(x)=-\frac{1}{\tau}\sum_{j=1}^{5}A_j \times\frac{\lambda_j[(1+\tau)(\lambda_j^2-m^2-\pi^2)-i\omega]}{(\lambda_j^2-m^2-\pi^2-i\omega/\tau)(\lambda_j^2-m^2-\pi^2-i\omega)} \times e^{\lambda_j x}. \tag{25d}$$

The five unknowns A_1, A_2, A_3, A_4 and A_5 are determined by the five boundary conditions imposed at $x=0$. A nontrivial solution exists if and only if a certain 5×5 determinant vanishes. This requirement yields a complex equation for the critical Rayleigh number $R(m)$ and the corresponding frequency $\omega(m)$ of the oscillations. Note that the limit $\Omega\to0$ is somewhat subtle since the dispersion relation then has a root $q_5=i\omega/\sigma+\mathcal{O}(\Omega^2)$. Consequently one must suppose that $A_5=\mathcal{O}(\Omega)$ before taking the limit $\Omega\to0$. The resulting equations then reduce to those studied in Ref. 6.

In Fig. 12 we show the precession frequencies and critical Rayleigh numbers as functions of the azimuthal wavenumber m for both retrograde modes ($\omega>0$) and prograde modes ($\omega<0$) for $\tau=0.067$, $\sigma=0.755$, $S=-0.3$ and several values of the rotation rate Ω. From the figures one can see that for low Ω a retrograde mode is selected while for larger Ω prograde modes are preferred. Note that since m is now a continuous variable the mode that is selected is the one corresponding to the minimum of the neutral stability curve $R(m)$.

Observe that the neutral stability curves extend over a limited range of m only. This range is narrow for small Ω, but increases as Ω increases. Outside the ranges shown there are no solutions satisfying the requirement of exponential fall-off as $x\to-\infty$, i.e., there are no solutions in the form of wall modes. The end points of the neutral stability curves are defined by the vanishing of one of the eigenvalues λ, indicating a transition to a body mode (cf. Ref. 6). Fig. 13 shows more detailed results for $\tau=0.067$, $\sigma=0.755$ and $\Omega=500$. As in Sec. III, among modes with a given m the retrograde modes are preferred for small $|S|$, but with increasing $|S|$ prograde modes are selected. Note that no prograde modes are present for sufficiently small $|S|$. For these parameter values Fig. 14 shows that as $|S|$ increases the minimum of the neutral curves as a function of m decreases. The figure shows that the minimum for the retrograde mode with $S=-0.03$ lies above that for the prograde mode with $S=-0.3$, although it is below the minimum for the retrograde mode at this value of S. Recall that for $S=-0.03$ there is no prograde mode at these parameter values. These results confirm the interpretation of these modes given in Sec. IV in terms of the class II modes of a stratified fluid in a rotating cylinder.

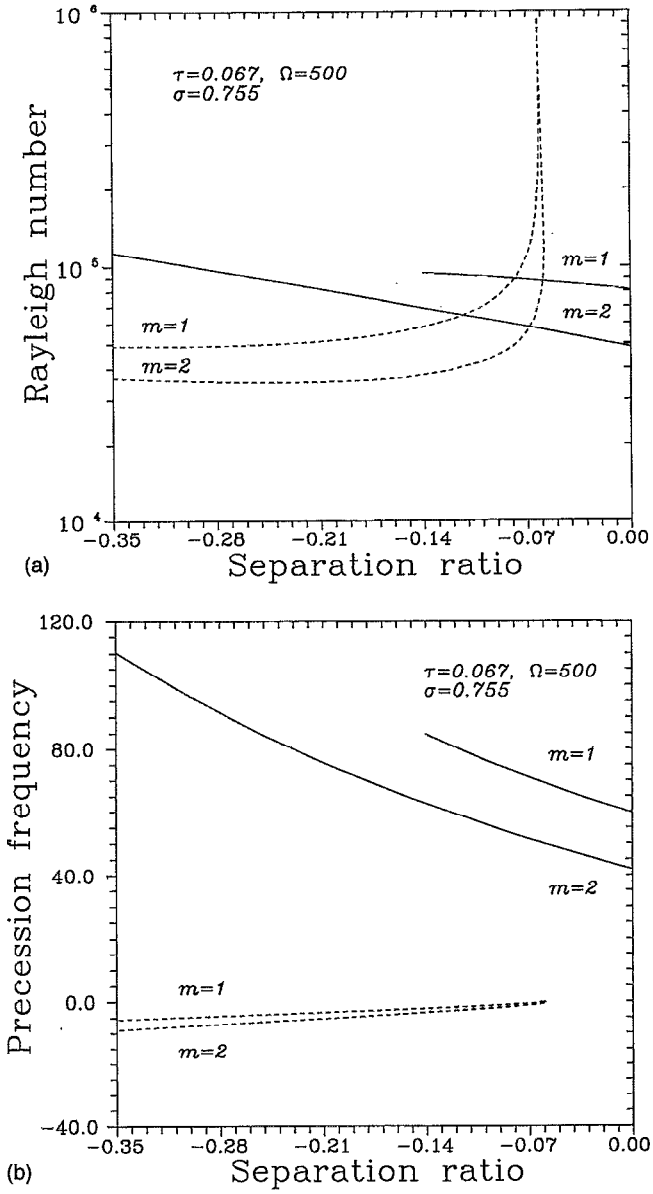

FIG. 13. As for Fig. 12 but showing (a) $R^{(m)}(S)$ and (b) $\omega^{(m)}(S)$ for $m=1,2$ when $\Omega=500$. Note that the prograde modes disappear at small $|S|$ leaving only retrograde modes.

The above results can also be used to check Acheson's picture of the destabilizing effect of negative separation ratios. For example, Fig. 13 shows that for $m=2$ the critical Rayleigh number $R_c^{(2)}$ reaches a minimum at $S=-0.23$. Acheson's criterion $\omega^{(2)}/p=1$ now yields $\ell=4.43$ which compares well with the inverse length computed from the dispersion relation (24) using the corresponding $\omega^{(2)}=-5.77$: $\ell=3.80$.

V. DISCUSSION AND CONCLUSION

In this paper we have presented detailed results for the onset of convection in binary mixtures in a rotating circular cylinder. These results are interesting and important for several reasons. We have found the system can support wall modes, and it is the presence of this new mode of instability

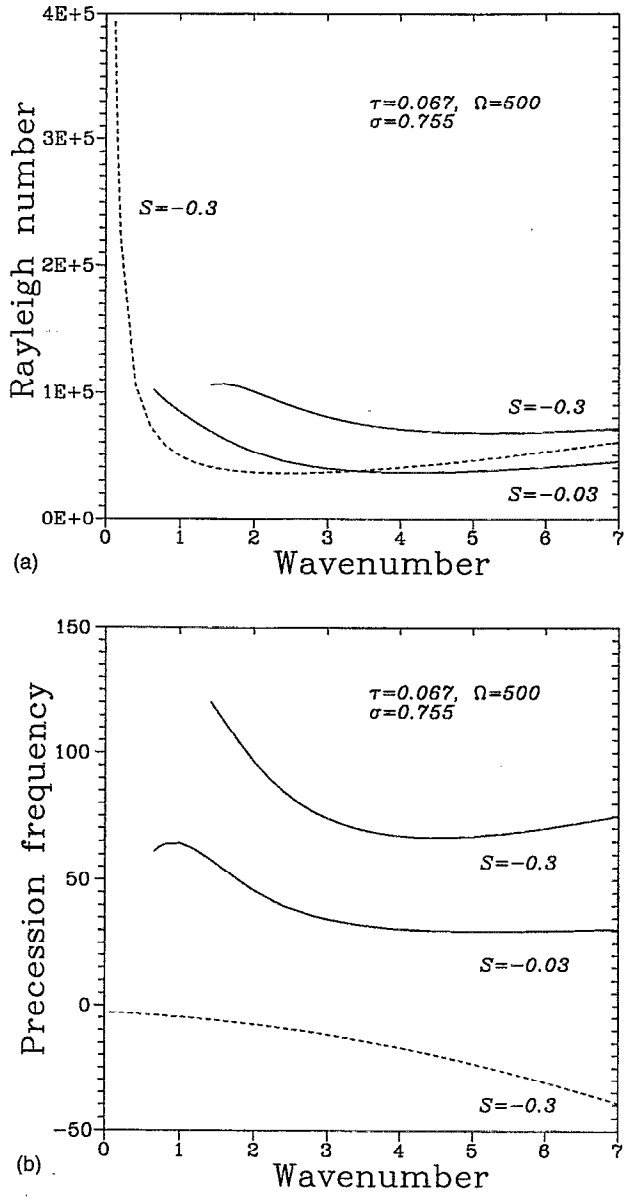

FIG. 14. As for Fig. 13 but showing the wavenumber dependence of the retrograde (solid line) and prograde (broken line) modes for $S=-0.3,-0.03$. (a) $R(m)$, and (b) $\omega(m)$. Note that there is no prograde mode when $S=-0.03$.

that is responsible for the fact that the critical Rayleigh numbers for the onset of nonaxisymmetric instability are in fact significantly lower than those for axisymmetric modes. This observation must be borne in mind when comparing experimental results with results based on calculations for an unbounded layer (cf. Ref. 8). We have seen that while these approximate the results for axisymmetric modes in a finite aspect ratio cylinder, particularly when the aspect ratio is large, they can grossly overestimate the actual critical Rayleigh number which typically corresponds to nonaxisymmetric modes. These effects are present even when the stabilizing stratification is weak ($|S|$ small) as is known from the pure fluid case. In binary fluids there is, however, an additional effect which makes the reduction in the critical Rayleigh number even more dramatic. This is the fact that the addition of an apparently stabilizing concentration gradient can in fact destabilize the system. This fact, first noted by Masuda[9] and Pearlstein,[10] is particularly pronounced when wall modes are involved. We found that although these modes have an entirely different physical character the explanation for this unexpected behavior proposed by Acheson[15] in the context of body modes applies to the wall modes as well. We believe that this observation, together with the detailed results presented above, may remove some of the longstanding discrepancies between measured and predicted critical Rayleigh numbers for this class of systems. As indicated by the analysis of the oscillation modes for a stably stratified ideal fluid in a rotating cylinder[21] the wall modes precess in the prograde direction and their precession speed is nearly independent of the rotation rate once this exceeds the buoyancy frequency. In contrast the wall modes in a pure fluid precess in the retrograde direction, while their frequency increases rapidly with the rotation rate. At cryogenic temperatures where visualization is difficult Nusselt number measurements usually provide the only information about the onset state. Regrettably since all steadily precessing states produce time-independent Nusselt numbers such measurements provide only limited data for comparison with theory.

ACKNOWLEDGMENTS

We are grateful to S. Friedlander and P. Lucas for helpful discussions. The work of M.N. and I.M. was supported by the Fundació Catalana per a la Recerca and DGICYT (Spain) under Grant No. PB91-0595 while that of E.K. was supported by an INCOR grant from Los Alamos National Laboratory.

[1]F. Zhong, R.E. Ecke, and V. Steinberg, "Rotating Rayleigh-Bénard convection: Küppers-Lortz transition," Physica D **51**, 596 (1991)
[2]R.E. Ecke, F. Zhong, and E. Knobloch, "Hopf bifurcation with broken reflection symmetry in rotating Rayleigh-Bénard convection," Europhys. Lett. **19**, 177 (1992).
[3]F. Zhong, R.E. Ecke, and V. Steinberg, "Rotating Rayleigh-Bénard convection: asymmetric modes and vortex states," J. Fluid Mech. **249**, 135 (1993).
[4]H.F. Goldstein, E. Knobloch, I. Mercader, and M. Net, "Convection in a rotating cylinder. Part 1. Linear theory for moderate Prandtl numbers," J. Fluid Mech. **248**, 583 (1993).
[5]H.F. Goldstein, E. Knobloch, I. Mercader, and M. Net, "Convection in a rotating cylinder. Part 2. Linear theory for low Prandtl numbers," J. Fluid Mech. **262**, 293 (1994).
[6]I. Mercader, M. Net, and E. Knobloch, "Binary fluid convection in a cylinder," Phys. Rev. E **51**, 339 (1995).
[7]E. Knobloch, "Bifurcations in rotating systems," in *Lectures on Solar and Planetary Dynamos*, edited by M.R.E. Proctor and A.D. Gilbert (Cambridge University Press, Cambridge, 1994), pp. 331–374.
[8]M.R. Ardron, P.G.J. Lucas, and N.D. Stein, "Exact calculation of convection thresholds in rotating binary liquid mixtures," Phys. Fluids A **4**, 664 (1992).
[9]A. Masuda, "Double diffusive convection in a rotating system," J. Oceanogr. Soc. Jpn. **34**, 8 (1978).
[10]A.J. Pearlstein, "Effect of rotation on the stability of a doubly diffusive fluid layer," J. Fluid Mech. **103**, 389 (1981).
[11]F. Marqués, M. Net, J.M. Massaguer, and I. Mercader, "Thermal convection in vertical cylinders. A method based on potentials of velocity," Comput. Appl. Mech. Eng. **110**, 157 (1993).
[12]I. Mercader, M. Net, and A. Falques, "Spectral methods for high order equations," Comput. Meth. Appl. Mech. Eng. **91**, 1245 (1991).
[13]P.G.J. Lucas, M.S. Thurlow, M.R. Ardron, J.K. Bhattacharjee, B.J. Ker-

shaw, M.D.J. Terrett, and A.L. Woodcraft, "Rayleigh-Bénard convection in rotating liquid ^{3}He-^{4}He mixtures," Physica B **194-196**, 841 (1994)
[14]M.S. Thurlow, "Rayleigh-Bénard convection in a rotating liquid ^{3}He-^{4}He mixture: The effects of Coriolis forces and a finite geometry," Ph.D. thesis, University of Manchester, 1993.
[15]D.J. Acheson, " 'Stable' density stratification as a catalyst for instability," J. Fluid Mech. **96**, 723 (1980).
[16]E. Knobloch, A. Deane, J. Toomre, and D.R. Moore, "Doubly diffusive waves," Contemp. Math. **56**, 203 (1986).
[17]A.E. Deane, E. Knobloch, and J. Toomre, "Travelling waves and chaos in thermosolutal convection," Phys. Rev. A **36**, 2862 (1987).
[18]E. Knobloch and D.R. Moore, "Linear stability of experimental Soret convection," Phys. Rev. A **37**, 860 (1988).
[19]J. Herrmann and F.H. Busse, "Asymptotic theory of wall-attached convection in a rotating fluid layer," J. Fluid Mech. **255**, 183 (1993).
[20]E.Y. Kuo and M.C. Cross, "Traveling-wave wall states in rotating Rayleigh-Bénard convection," Phys. Rev. E. **47**, R2245 (1993).
[21]S. Friedlander and W.L. Siegmann, "Internal waves in a contained rotating stratified fluid," J. Fluid Mech. **114**, 123 (1982).
[22]T. Clune and E. Knobloch, "Pattern selection in rotating convection with experimental boundary conditions," Phys. Rev. E **47**, 2536 (1993).
[23]E. Knobloch, "Convection in binary fluids," Phys. Fluids **23**, 1918 (1980).